International Conference and Early Career Scientists School on Environmental Observations, Modeling and Information Systems
ENVIROMIS-2010, 5-11 July 2010, Tomsk, Russia

Supercomputer Technologies for Modeling Climate Change

V.N. Lykosov
Institute for Numerical Mathematics, RAS
M.V. Lomonosov Moscow State University
E-mail: lykossov@inm.ras.ru

Goal and main objectives of climate modeling

Goal: development of (e.g. national) expert system for scientifically grounded forecasts of climate change on global and regional scales and for assessing consequences of climate change for environment and human society.

Main objectives:

1. the reproduction of the present-day climate (understanding physics of climate);
2. the assessment of possible climate changes under the influence of small external forcing (sensitivity of the climate system);
3. the forecast of climate change and assessing its impact on environment and society.

Objectives of climate modeling

- **To reproduce both "climatology" (seasonal and monthly means) and statistics of variability: intra-seasonal (monsoon cycle, characteristics of storm-tracks, etc.) and climatic (dominated modes of inter-annual variability such as El-Nino phenomenon or Arctic Oscillation)**

- **To estimate climate change due to anthropogenic activity**

- **To reproduce with high degree of details regional climate: features of hydrological cycle, extreme events, impact of global climate change on regional climate, environment and socio-economic relationships**

Regional scale modeling and assessment

- **Atmospheric modeling, e.g. using global climate model with improved spatial resolution in the region under consideration and non-hydrostatic mesoscale models: parameterization of mesoscale variability**

- **Vegetation modeling, e.g. models of vegetation dynamics: parameterization of biogeochemical and hydrological cycles**

- **Soil (including permafrost) modeling, e.g. models of snow and frozen ground mechanics: parameterization of hydrological and biogeochemical cycles**

Regional scale modeling and assessment

- **Catchment modeling, e.g. constructing models of river and lakes dynamics: parameterization of hydrological cycle**

- **Coupled regional models**

- **Air and water quality modeling**

- **Statistical and dynamic downscaling (e.g. regional projections of global climate change patterns)**

Michel Desgagné (Reading, 13 HPC Workshop, 3-7/11/2008)
High performance computing at the Canadian Meteorological Centres

Uninterrupted (24/7, year-round) weather and environmental forecasts, serving public and military needs of Canadians

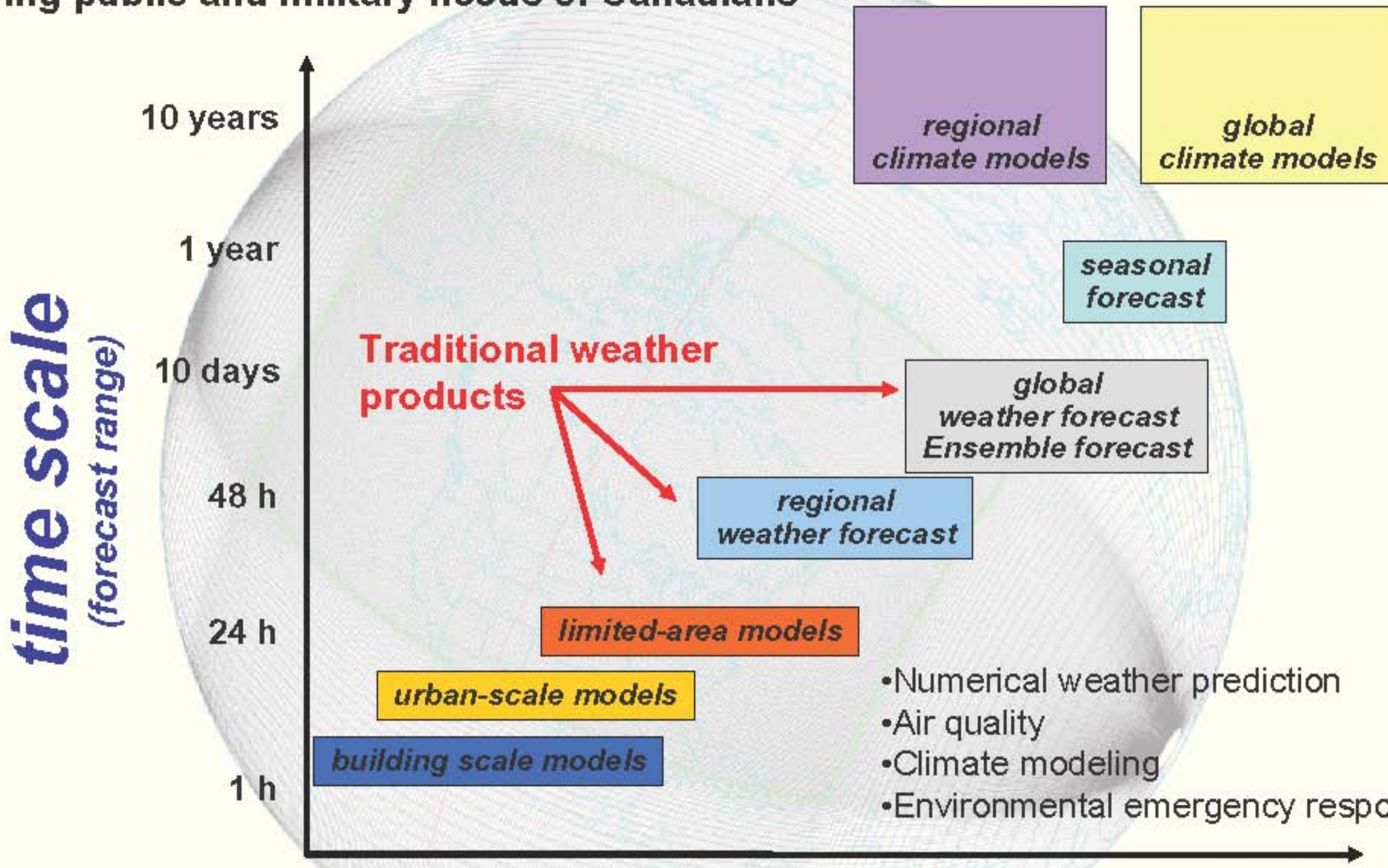

- Numerical weather prediction
- Air quality
- Climate modeling
- Environmental emergency response

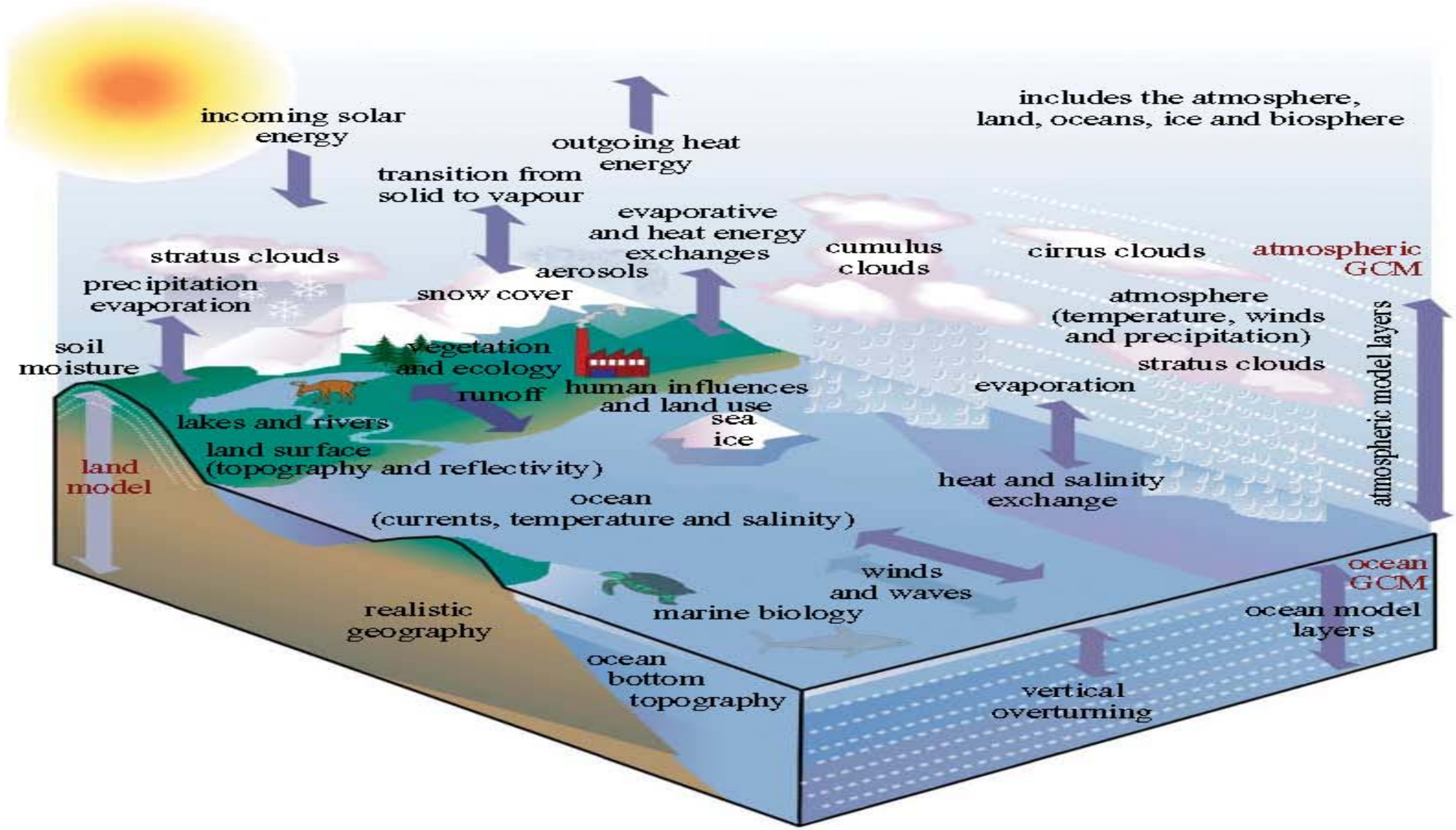

Figure 1. Schematic of the components of the NCAR Community Climate System Model, which is supported by the National Science Foundation (NSF) and the Department of Energy (DOE). Adapted from Kevin Trenberth (NCAR). GCM is an acronym for general circulation model. Copyright © University Corporation for Atmospheric Research. Illustration by Paul Grabhorn.

Towards Comprehensive Earth System Models

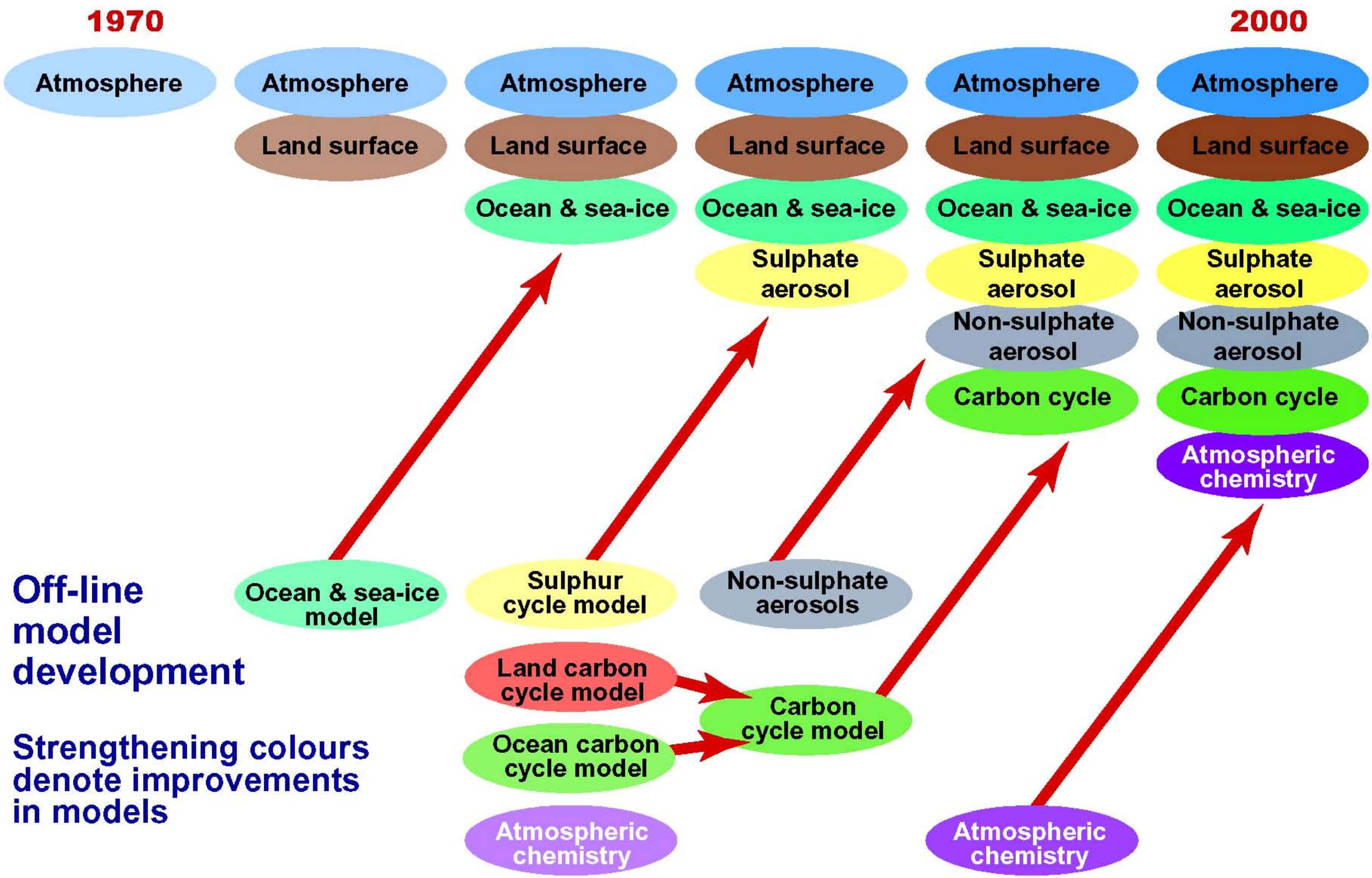

General CirculationModel of the Atmosphere and Ocean
Novosibirsk Computer Center
(Marchuk et al., 1980)

- **Coupled model based on the implicit scheme and splitting-up method in time. Synchronization of thermal relaxation times (1 «atmospheric» year = 100 «oceanic» years). The atmospheric resolution: 10x6 degrees in longitude and latitude, 3 levels in vertical up to 14 km (3240 grid points). Time step: 40 min. The oceanic resolution: 5x5 degrees and 4 levels (7200 grid points). Time step: 2 days.**

- **A single experiment: mean-January circulation, for calculations on 40 model «atmospheric» days (11 «oceanic» years) about three months of real time on BESM-6 computer are spent.**

BESM-6

Mean performance – up to 1 Mflop/s

Frequency – 10 MHz , RAM – 32768 words

Climate model
Institute for Numerical Mathematics, RAS
(Dymnikov et al., 2005, Volodin and Diansky, 2006, http://ksv.inm.ras.ru/index)

- **Coupled model. Atmospheric resolution: 2.5x2 degrees in longitude and latitude, 21 levels in vertical up to 30 km (272160 grid points). Time step: 6 min. Oceanic resolution: 1x0.5 degrees, 40 levels (3425600 grid points). Time step: 2 hours.**

- **A set of experiments for modeling the present-day climate and assessing climate change in the future (integration for 200 – 500 years) for the 5-th IPCC Report contribution (2013).**

- **Calculations for 8 years of model time require 1 day of real time. Thus, to carry out 1 numerical experiment 1 - 2 months of real time should be spent.**

Supercomputer SKIF MSU - Chebyshev

60 Tflop/s, 1250 processors Intel Xeon (*4 kerns)

T. Reichler, J. Kim. How well do coupled models simulate today's climate? – BAMS, 2008, 303 – 311.

TABLE 1. Climate variables and corresponding validation data. Variables listed as "zonal mean" are latitude–height distributions of zonal averages on twelve atmospheric pressure levels between 1000 and 100 hPa. Those listed as "ocean," "land," or "global" are single-level fields over the respective regions. The variable "net surface heat flux" represents the sum of six quantities: incoming and outgoing shortwave radiation, incoming and outgoing longwave radiation, and latent and sensible heat fluxes. Period indicates years used to calculate observational climatologies.

Variable	Domain	Validation data	Period
Sea level pressure	ocean	ICOADS (Woodruff et al. 1987)	1979–99
Air temperature	zonal mean	ERA-40 (Simmons and Gibson 2000)	1979–99
Zonal wind stress	ocean	ICOADS (Woodruff et al. 1987)	1979–99
Meridional wind stress	ocean	ICOADS (Woodruff et al. 1987)	1979–99
2-m air temperature	global	CRU (Jones et al. 1999)	1979–99
Zonal wind	zonal mean	ERA-40 (Simmons and Gibson 2000)	1979–99
Meridional wind	zonal mean	ERA-40 (Simmons and Gibson 2000)	1979–99
Net surface heat flux	ocean	ISCCP (Zhang et al. 2004), OAFLUX (Yu et al. 2004)	1984 (1981) –99
Precipitation	global	CMAP (Xie and Arkin 1998)	1979–99
Specific humidity	zonal mean	ERA-40 (Simmons and Gibson 2000)	1979–99
Snow fraction	land	NSIDC (Armstrong et al. 2005)	1979–99
Sea surface temperature	ocean	GISST (Parker et al. 1995)	1979–99
Sea ice fraction	ocean	GISST (Parker et al. 1995)	1979–99
Sea surface salinity	ocean	NODC (Levitus et al. 1998)	variable

on a grid-point basis with the observed interannual variance, and averaging globally. In mathematical terms this can be written as

$$e_{vm}^2 = \sum_n \left(w_n \left(\bar{s}_{vmn} - \bar{o}_{vn} \right)^2 / \sigma_{vn}^2 \right), \qquad (1)$$

where $\bar{s}_{vmn}$ is the simulated climatology for climate variable (v), model (m), and grid point (n); $\bar{o}_{vn}$ is the corresponding observed climatology; w_n are proper weights needed for area and mass averaging; and σ_{vn}^2 is the interannual variance from the validating observations. The normalization with the interannual variance helped to homogenize errors from different regions and variables. In order to ensure that different climate variables received similar weights when combining their errors, we next scaled e^2 by the average error found in a reference ensemble of models—that is,

$$I_{vm}^2 = e_{vm}^2 \Big/ \overline{e_{vm}^2}^{m=20C3M}, \qquad (2)$$

where the overbar indicates averaging. The reference ensemble was the present-day CMIP-3 experiment. The final model performance index was formed by taking the mean over all climate variables (Table 1) and one model using equal weights,

$$I_m^2 = \overline{I_{vm}^2}^{v}. \qquad (3)$$

The final step combines the errors from different climate variables into one index. We justify this step by normalizing the individual error components prior to taking averages [Eqs. (1) and (2)]. This guarantees that each component varies evenly around one and has roughly the same variance. In this sense, the individual I_{vm}^2 values can be understood as rankings with respect to individual climate variables, and the final index is the mean over all ranks. Note that a very similar approach has been taken by Murphy et al. (2004).

RESULTS. The outcome of the comparison of the 57 models in terms of the performance index I^2 is illustrated in the top three rows of Fig. 1. The I^2 index varies around one, with values greater than one for underperforming models and values less than one

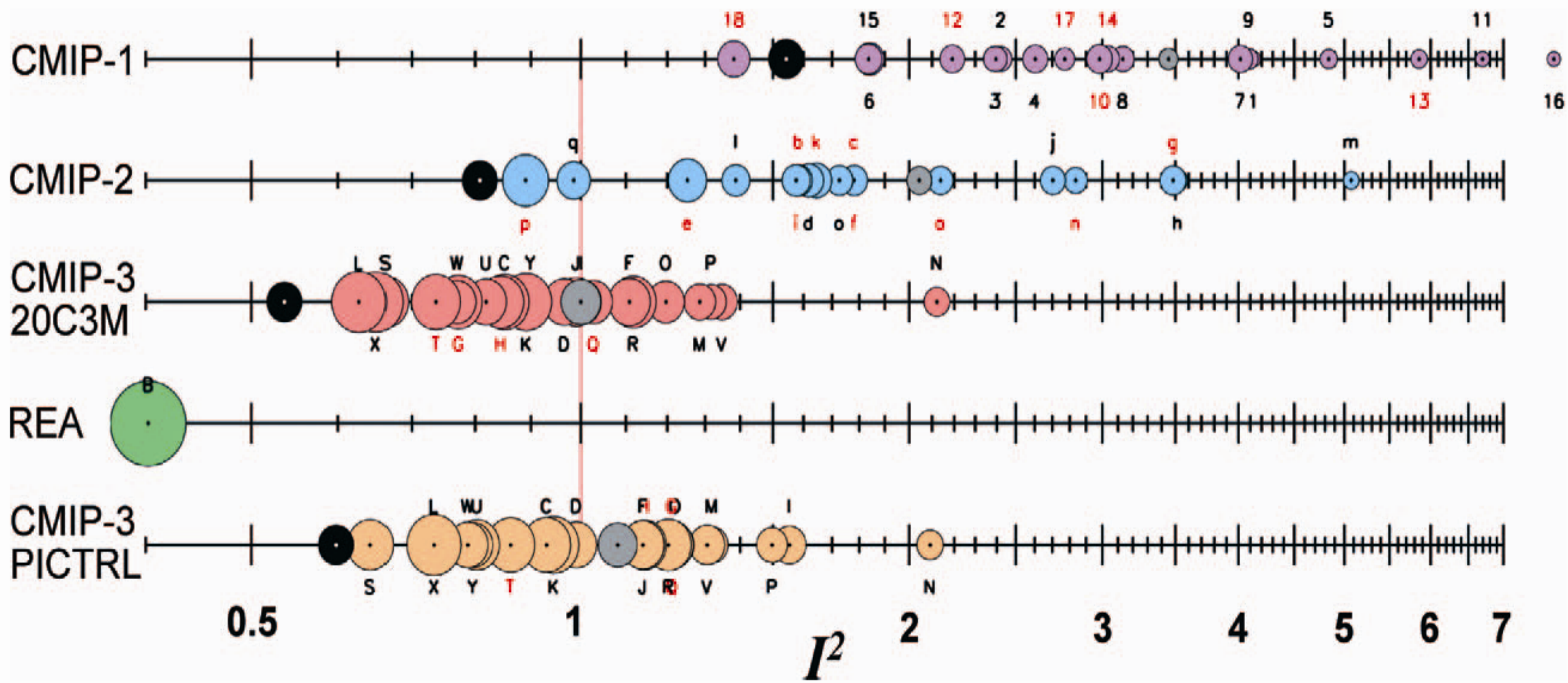

FIG. 1. Performance index I^2 for individual models (circles) and model generations (rows). Best performing models have low I^2 values and are located toward the left. Circle sizes indicate the length of the 95% confidence intervals. Letters and numbers identify individual models (see supplemental online material at doi:10.1175/BAMS-89-3-Reichler); flux-corrected models are labeled in red. Grey circles show the average I^2 of all models within one model group. Black circles indicate the I^2 of the multimodel mean taken over one model group. The green circle (REA) corresponds to the I^2 of the NCEP/NCAR reanalyses. Last row (PICTRL) shows I^2 for the preindustrial control experiment of the CMIP-3 project.

During the last 30 years the performance of supercomputers increased 10^6 times (from 10^6 to 10^{12} Flop/s).

Computational expenses to carry out numerical experiments for modeling climate and climate change are also nearly 10^6 times increased (mainly, due to long-term – up to hundreds model years – simulations).

Now, ensemble calculations (with the sample length – up to 10^3 numerical experiments) are claimed and this requires the use of petaflop supercomputers.

The horizontal resolution of the majority of climate models, results of which were used in the 4-th IPCC Report (2007) is about 200 km.

The progress achieved in the development of supercomputers and computational technologies suggests that the climate modeling community is now ready to start with the development of models, the typical resolution of which is enough to explicitly describe mesoscale (2 – 200 km) non-hydrostatic processes on the whole Earth.

WCRP
World Climate Research Programme

World Modelling Summit for Climate Prediction

WMO UNESCO IOC ICSU International Council for Science

ECMWF, Reading, May 6 – 9, 2008

http://www.ecmwf.int/publications/cms/get/ecmwfnews/1213113497484

Revolutionary Perspective: from climate models to Earth System Models

Challenges for the Future

Based on P. Cox, 2004

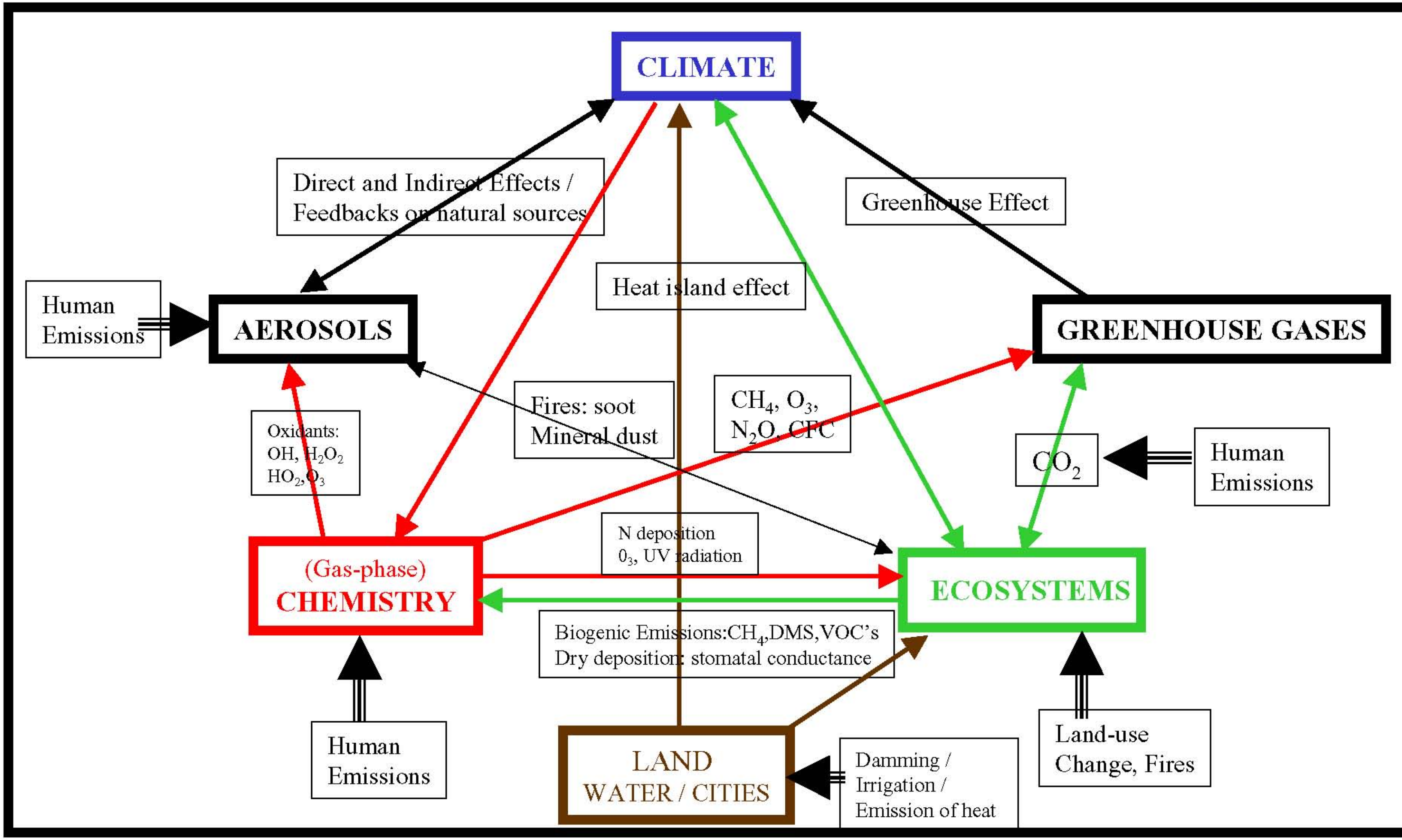

The future: a full treatment of climate-chemistry-ecosystem-land surface feedbacks

CLM4 – First (zero) generation land component of ESM

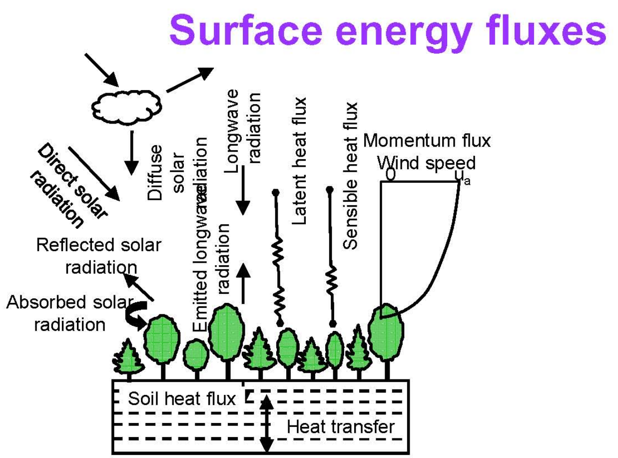

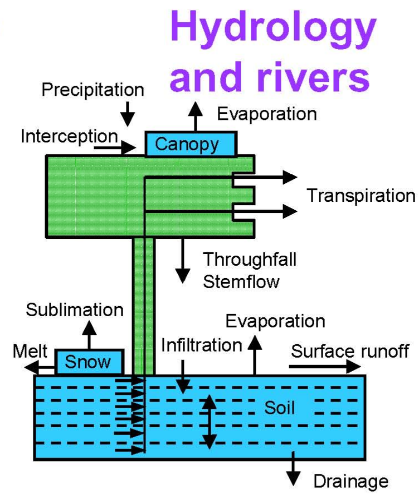

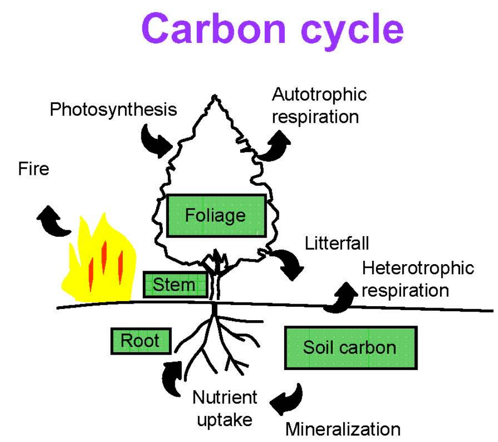

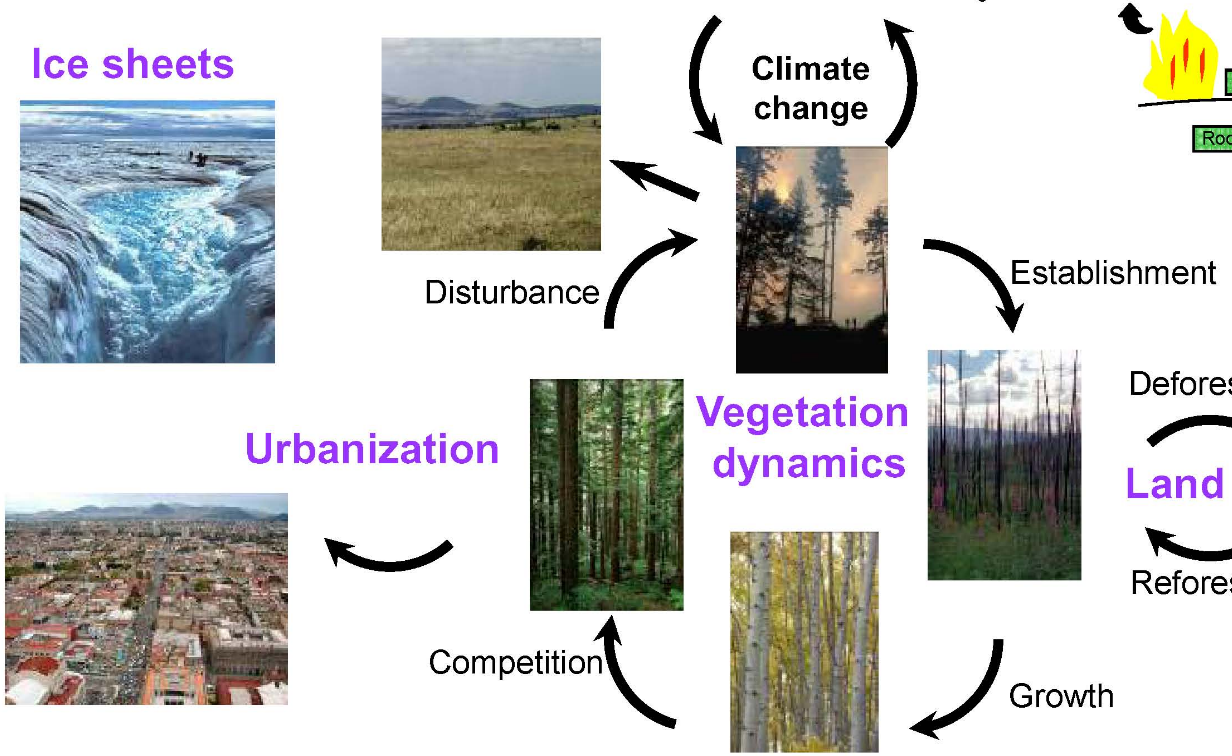

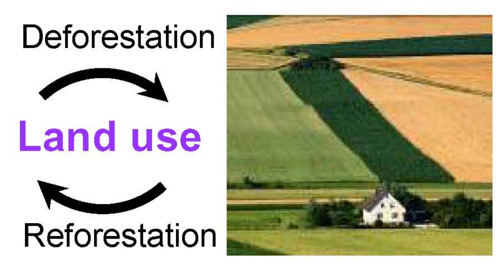

Earth System Model

R. Loft. The Challenges of ESM Modeling at the **Petascale**

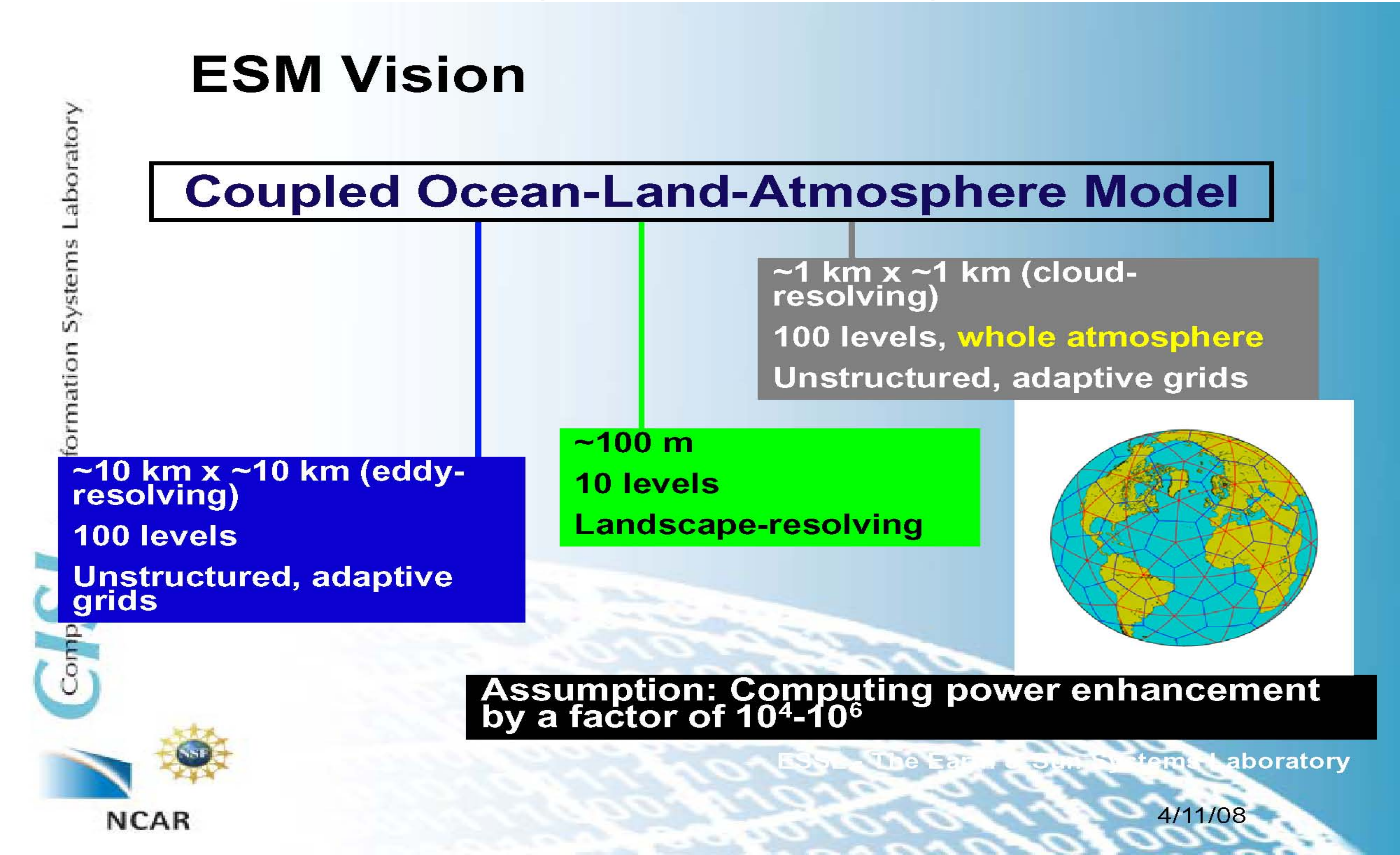

Petaflop with ~1M Cores By 2008

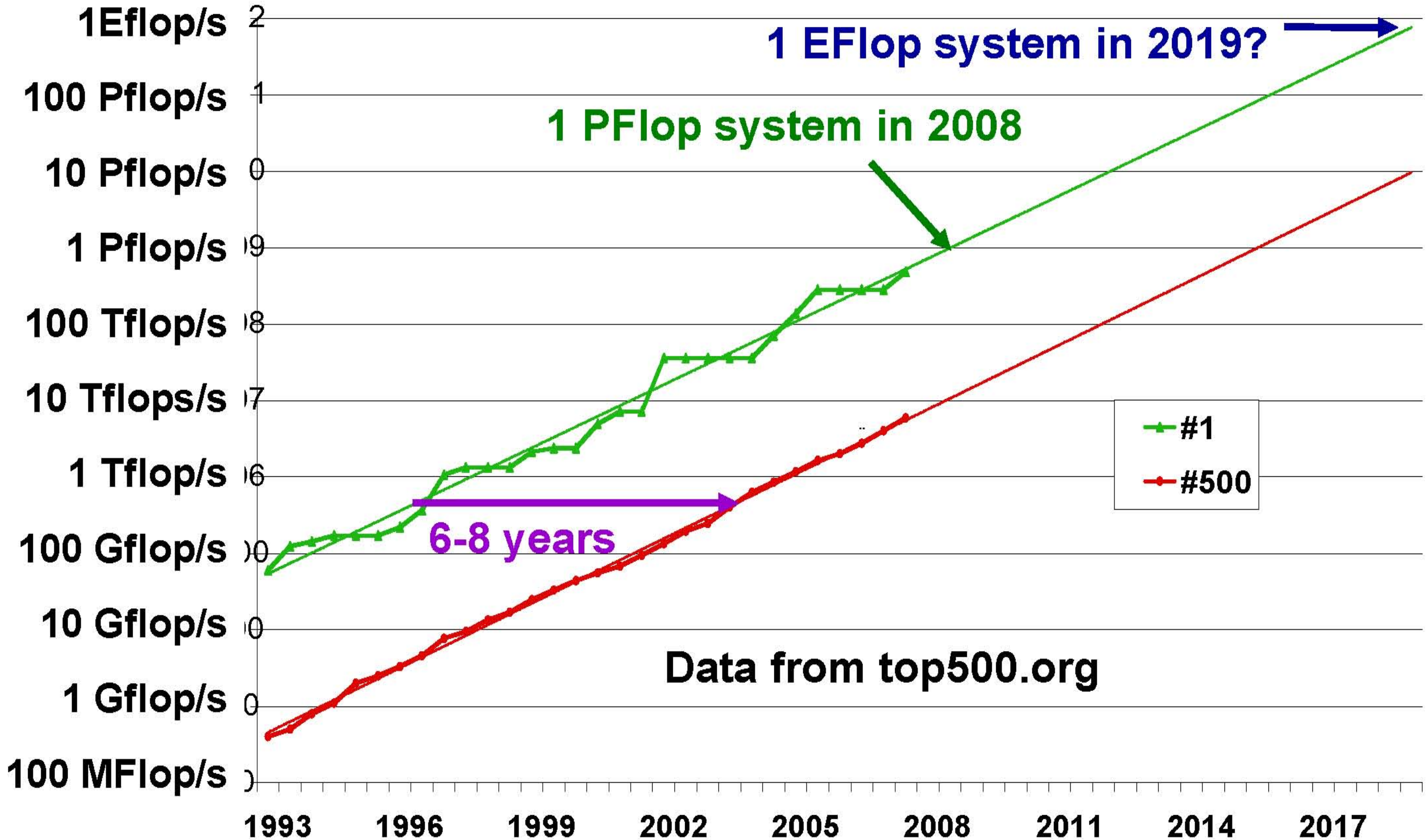

Slide source Horst Simon, LBNL

Суперкомпьютер МГУ “Ломоносов”

Lomonosov supercomputer key features

Peak and real performance	420 Tflops, 350 Tflops
Linpack efficiency	83%
Number of compute nodes	4 446
Number of processors	8 892
Number of processor cores	35 776
Primary and secondary compute nodes	T-Blade2; T-Blade1.1, PeakCell S
Processor type of primary and secondary compute nodes	Intel® Xeon X5570; Intel® Xeon X5570, PowerXCell 8i
Total RAM	56 TB
Primary interconnect	QDR Infiniband
Secondary interconnect	10G Ethernet, Gigabit Ethernet
External storage	up to 1 350TB,
Operating system	Clustrx T-Platforms Edition
Total area	252 square meters
Power consumption (supercomputer)	1.5MW

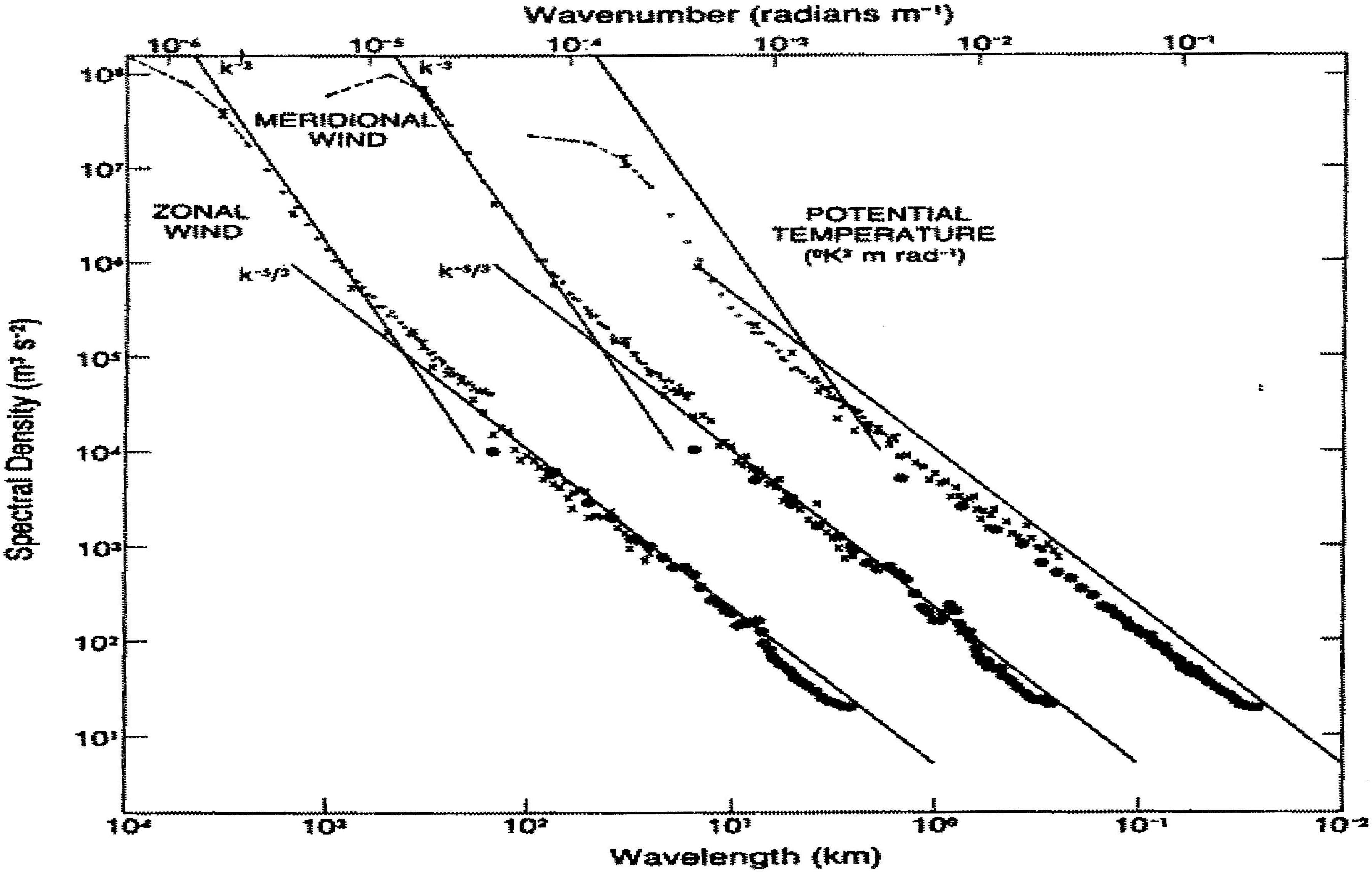

FIG. 1. Variance power spectra of wind and potential temperature near the tropopause from GASP aircraft data. The spectra for meridional wind and temperature are shifted one and two decades to the right, respectively; lines with slopes -3 and $-5/3$ are entered at the same relative coordinates for each variable for comparison. [Reproduced with permission from Nastrom and Gage (1985).]

TECHNICAL MEMORANDUM

31

On the relation between index cycles of the atmosphere circulation and spatial spectrum of the kinetic energy in the model of the general circulation of the atmosphere

G.I.Marchuk, V.P. Dymnikov and V.N. Lykossov

Research Department

May 1981

European Centre for Medium-Range Weather Forecasts
Europäisches Zentrum für mittelfristige Wettervorhersage
Centre européen pour les prévisions météorologiques à moyen

Large-scale hydro-thermodynamics of the atmosphere

$$\frac{du}{dt} - \left(f + \frac{u}{a}\mathrm{tg}\varphi \right) v + \frac{1}{a\cos\varphi}\left(\frac{\partial \Phi}{\partial \lambda} + \frac{RT}{\pi}\frac{\partial \pi}{\partial \lambda} \right) = F_u \,,$$

$$\frac{dv}{dt} + \left(f + \frac{u}{a}\mathrm{tg}\varphi \right) u + \frac{1}{a}\left(\frac{\partial \Phi}{\partial \varphi} + \frac{RT}{\pi}\frac{\partial \pi}{\partial \varphi} \right) = F_v \,,$$

$$\frac{\partial \Phi}{\partial \sigma} = -\frac{RT}{\sigma} \,,$$

$$\frac{\partial \pi}{\partial t} + \frac{1}{a\cos\varphi}\left(\frac{\partial \pi u}{\partial \lambda} + \frac{\partial \pi v \cos\varphi}{\partial \varphi} \right) + \frac{\partial \pi \dot{\sigma}}{\partial \sigma} = 0 \,,$$

$$\frac{dT}{dt} - \frac{RT}{c_p \sigma \pi}\left[\pi\dot{\sigma} + \sigma\left(\frac{\partial \pi}{\partial t} + \frac{u}{a\cos\varphi}\frac{\partial \pi}{\partial \lambda} + \frac{v}{a}\frac{\partial \pi}{\partial \varphi} \right) \right] = F_T + \varepsilon \,,$$

$$\frac{dq}{dt} = F_q - (C - E),$$

where $$\frac{d}{dt} = \frac{\partial}{\partial t} + \frac{u}{a\cos\varphi}\frac{\partial}{\partial \lambda} + \frac{v}{a}\frac{\partial}{\partial \varphi} + \dot{\sigma}\frac{\partial}{\partial \sigma} \,.$$

Subgrid-scale processes: parameterization

2.2 Small-scale diffusion

The rates of change of momentum, temperature and moisture caused by small-scale diffusion consist of two parts, $F = F^H + F^V$, where subscripts H and V denote the contributions of horizontal diffusion and vertical mixing, respectively. The vertical diffusion and its parameterization in model have been described above.

The horizontal turbulent small-scale diffusion must not affect the total angular momentum of the system. This imposes certain constraints on finite-difference approximations of diffusive terms satisfying dissipative conditions and the conservation of global angular momentum if these terms are represented as

$$F_u^H = \frac{1}{a^2\cos^2\phi p_s}\left[\frac{\partial}{\partial\lambda} p_s K_H \frac{\partial u}{\partial\lambda} + \frac{\partial}{\partial\phi} p_s K_H \cos^3\phi \frac{\partial \frac{u}{\cos\phi}}{\partial\phi}\right] \tag{20a}$$

$$F_s^H = \frac{1}{a^2\cos^2\phi p_s}\left[\frac{\partial}{\partial\lambda} p_s K_H \frac{\partial s}{\partial\lambda} + \cos\phi \frac{\partial}{\partial\phi} p_s K_H \cos\phi \frac{\partial s}{\partial\phi}\right] \tag{20b}$$

where S = v, T, q. In (20) K_H is the horizontal diffusion coefficient, which where S = v, T, q. In (20) K_H is the horizontal diffusion coefficient, which has been chosen as follows (Smagorinsky, 1963):

$$K_M = \mu[K_H^o + l^2 \sqrt{D_T^2 + D_S^2}] \tag{21}$$

where

$$D_T = \frac{1}{a\cos\phi}\frac{\partial u}{\partial\lambda} - \frac{\cos\phi}{a}\frac{\partial}{\partial\phi}\left(\frac{v}{\cos\phi}\right) \tag{22a}$$

$$D_S = \frac{1}{a\cos\phi}\frac{\partial V}{\partial\lambda} + \frac{\cos\phi}{a}\frac{\partial}{\partial\phi}\left(\frac{u}{\cos\phi}\right) \tag{22b}$$

$$l^2 = 0.08\ a^2(\cos^2\phi\ \Delta\lambda^2 + \Delta\phi^2) \tag{22c}$$

($\Delta\lambda$ and $\Delta\phi$ are parameters of the grid domain)

$$K_H^o = \text{const} = 50000\ m^2/\text{sec} \tag{22d}$$

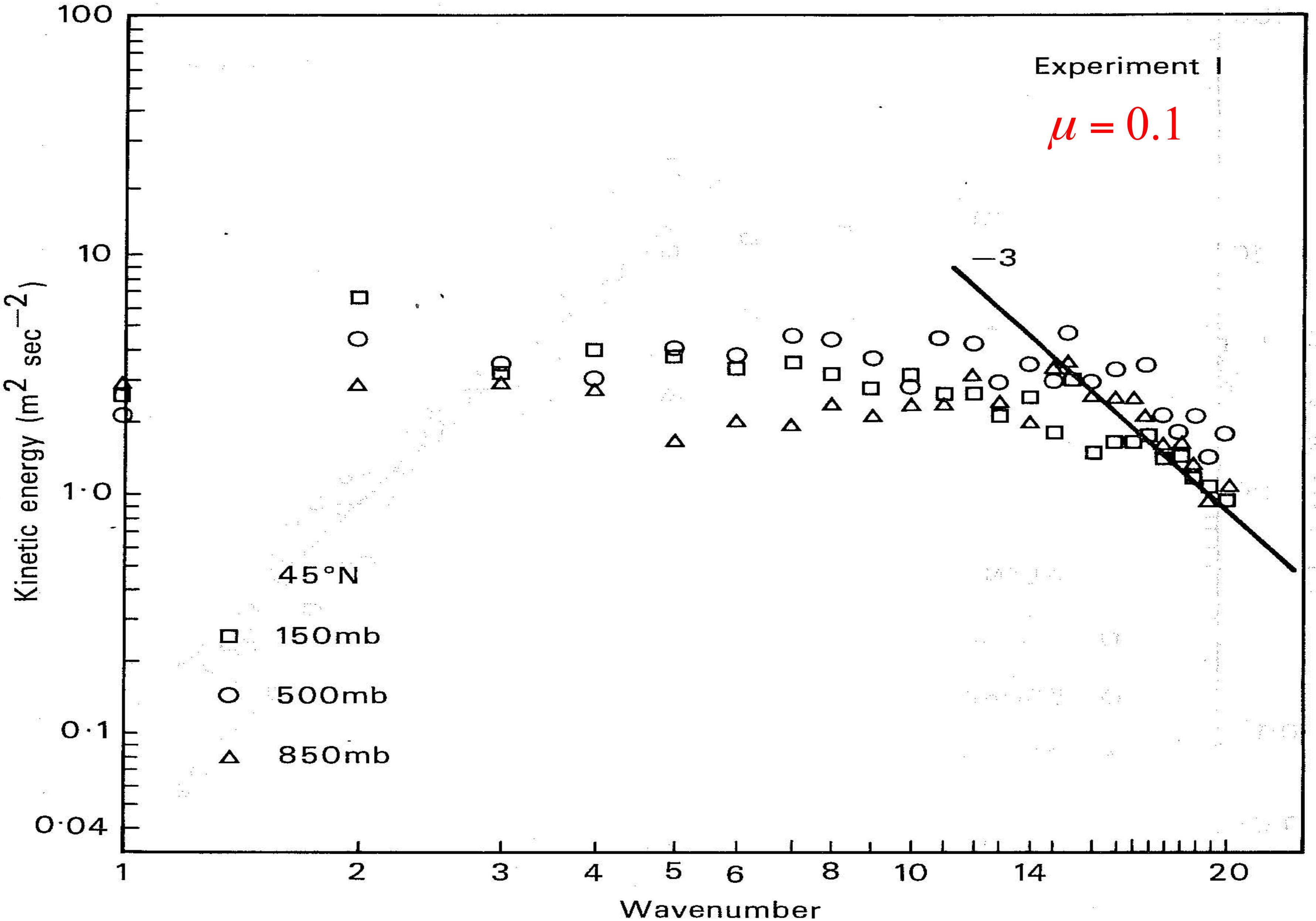

Fig. 2 Spectral distribution of eddy kinetic energy at 45°N (Experiment I).

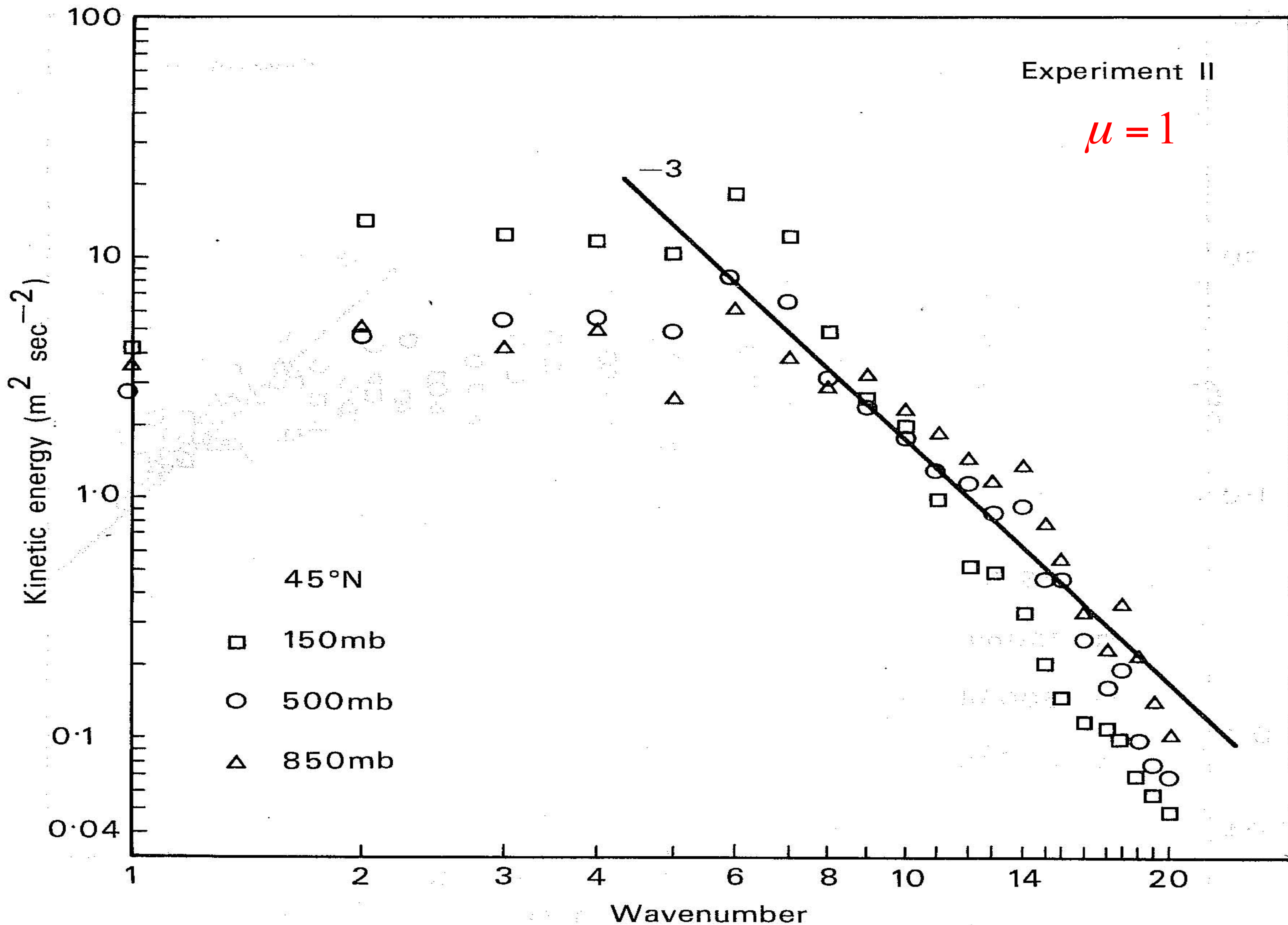

Fig. 3 Same as Fig. 2 but for Experiment II.

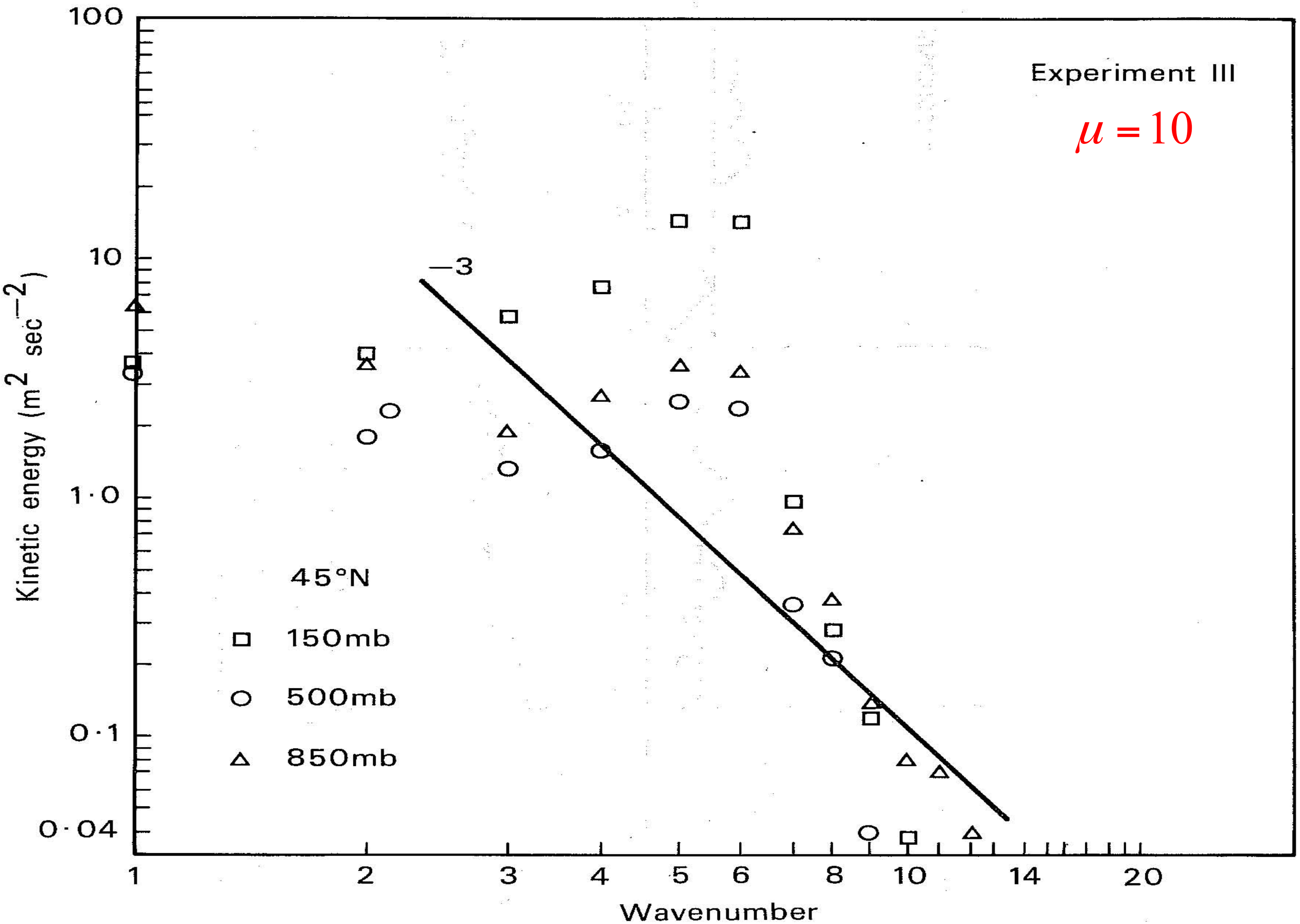

Fig. 4 Same as Fig. 2 but for Experiment III.

Working out of the multiscale modelling systems will be the key moment of the further development of climate models, their ability to reproduce features of an observable spatial spectra of kinetic and available potential energy can serve one of criteria of models quality.

Koshyk and Hamilton (2001): the GFDL GCMA (USA) with the horizontal resolution about 35 km => in troposphere spectral distribution of the calculated kinetic energy corresponds to the degree law «-3» on scales from 5000 to 500 km and to the degree law «-5/3» on smaller scales. In a stratosphere and mesosphere similar distributions, but transition from one law to another took place on scales of 2000 and 4000 km, accordingly, that contradicts the observed data and can testify to parameterization lacks of sub-grid-scale processes.

Experiments with regional model WRF (Skamarock, 2004) at various horizontal resolution (22, 10 and 4 km, accordingly): the calculated spectra well coincide in a meso-scale range with observed ones, including transition from an exponent «-5/3» to degree «-3». However the modelled spectrum in its short-wave part has appeared strongly depending on properties of computational technology (in particular, from level of the scheme dissipation).

Mesoscale processes

- **Weather systems smaller than synoptic scale systems (~ 1000 and more km) but larger than microscale (< 1 km) and storm-scale (~ 1 km) cumulus systems.**
- **Horizontal dimensions: from about 2 km to several hundred kilometers.**
- **Examples of mesoscale weather systems: sea and lake breezes, squall lines, katabatic flows, mesoscale convective complexes.**
- **Vertical velocity equals or exceeds horizontal velocities in mesoscale meteorological systems due to non-hydrostatic processes.**

Structure of Cloud Cluster in the Tropics

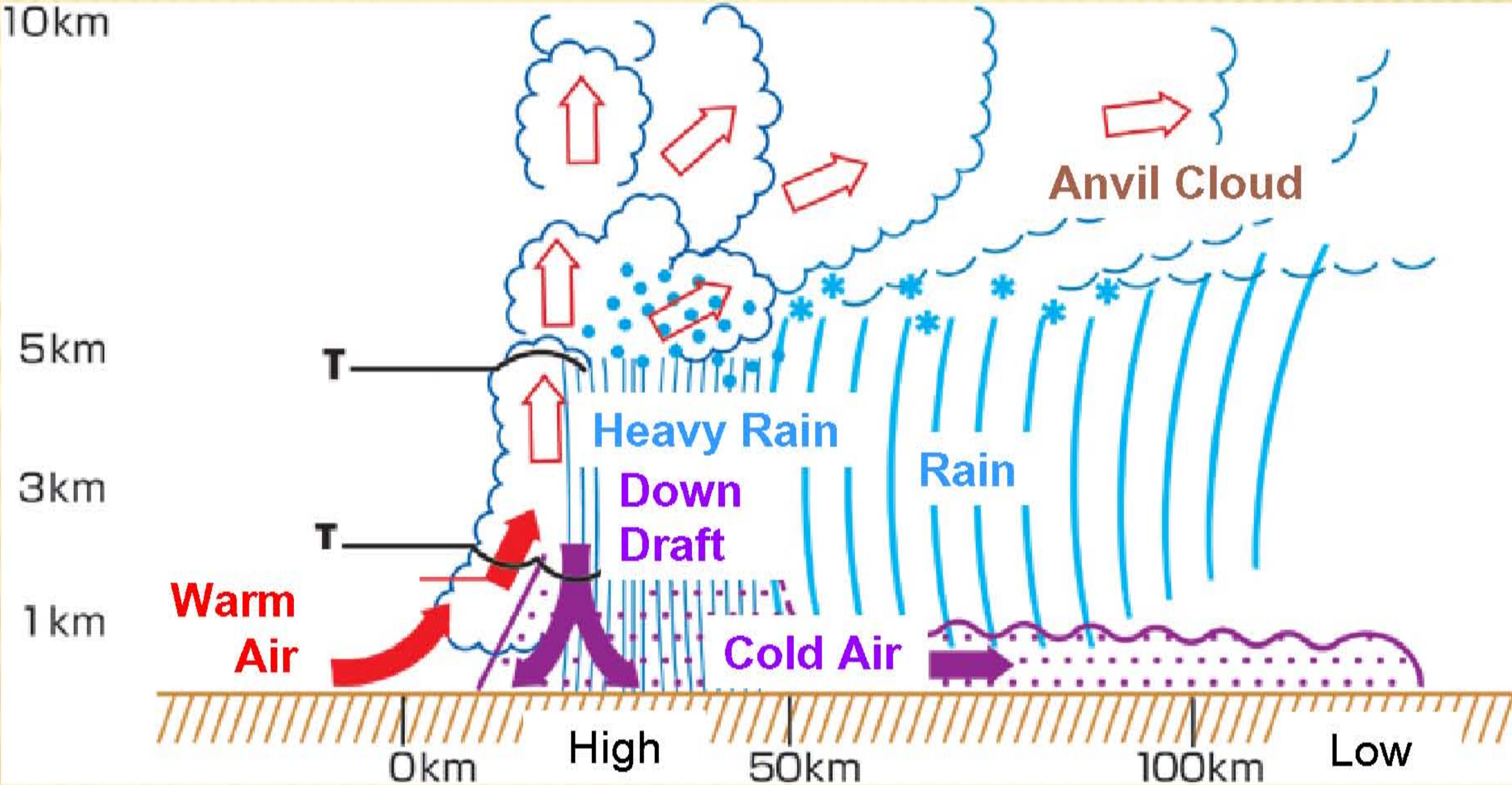

Cloud Streets (R. Rotunno, 2007)

Synoptic variations

Boundary-Layer turbulence

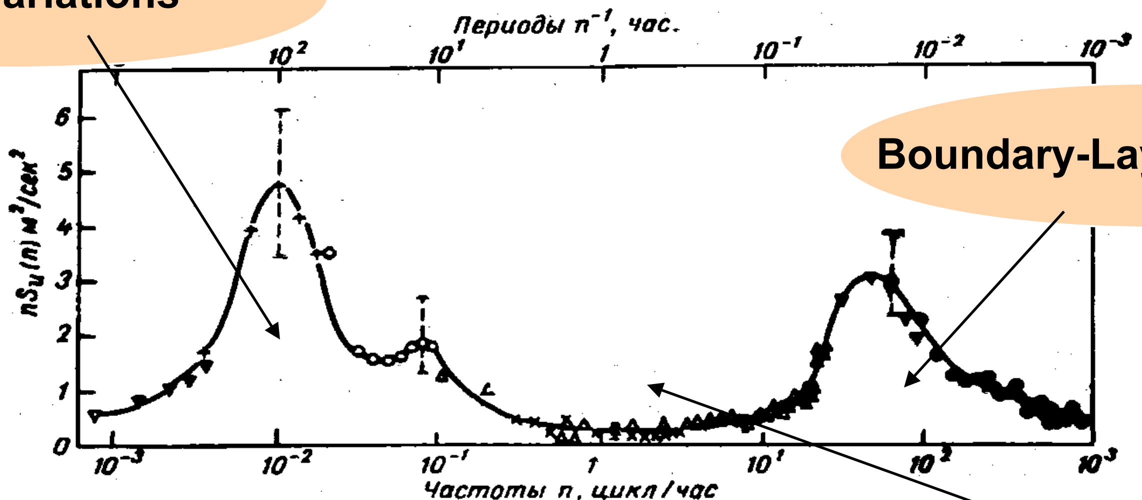

Спектр скорости ветра в приземном слое атмосферы (по Ван дер Ховену (1957), n — частота, $S_u(n)$ — спектральная плотность.

Mesoscale processes

Energy range

Inertial range

$E(k) \cong \varepsilon^{2/3} k^{-5/3}$

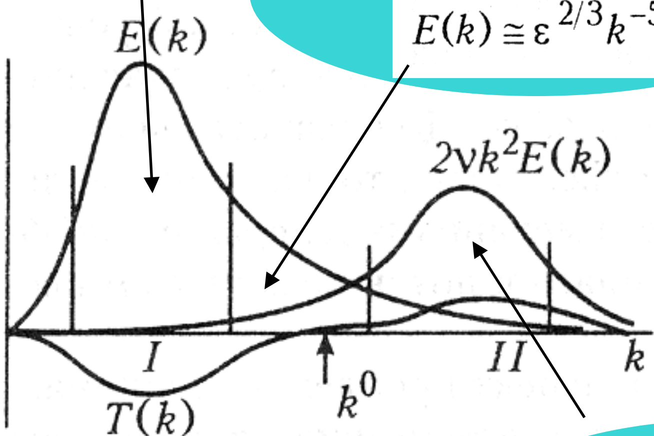

Dissipation range

$$a(x_i,t) = \tilde{a}(x_i,t) + a'(x_i,t) + a''(x_i,t)$$

$$\overline{a}(x_i,t) = \int G(x_i - x_i')a(x_i',t)dx_i'$$

$$\overline{a}(x_i,t) = \tilde{a}(x_i,t) + a'(x_i,t)$$

Mesoscale atmospheric model
(Miranda, 1991, Stepanenko et al., 2006)

$$\frac{\partial u p_*}{\partial t}+\frac{\partial u^2 p_*}{\partial x}+\frac{\partial v u p_*}{\partial y}+\frac{\partial \dot{\sigma} u p_*}{\partial \sigma}=-p_*\frac{\partial \phi'}{\partial x}+\sigma\frac{\partial p_*}{\partial x}\frac{\partial \phi'}{\partial \sigma}+(fv-\tilde{f}\tilde{w})p_*+p_*D_u,$$

$$\frac{\partial v p_*}{\partial t}+\frac{\partial u v p_*}{\partial x}+\frac{\partial v^2 p_*}{\partial y}+\frac{\partial \dot{\sigma} v p_*}{\partial \sigma}=-p_*\frac{\partial \phi'}{\partial y}+\sigma\frac{\partial p_*}{\partial y}\frac{\partial \phi'}{\partial \sigma}-fup_*+p_*D_v,$$

$$\frac{\partial \tilde{w} p_*}{\partial t}+\frac{\partial u \tilde{w} p_*}{\partial x}+\frac{\partial v \tilde{w} p_*}{\partial y}+\frac{\partial \dot{\sigma} \tilde{w} p_*}{\partial \sigma}=-S_v p_*\frac{\partial \phi'}{\partial \sigma}-p_* g\frac{\rho'}{\rho_s}+\tilde{f}up_*+p_*D_w,$$

$$\frac{\partial p_*}{\partial t}+\frac{\partial u p_*}{\partial x}+\frac{\partial v p_*}{\partial y}+\frac{\partial \dot{\sigma} p_*}{\partial \sigma}=0,$$

$$\frac{\rho'}{\rho_s}=-\left(\frac{\theta'}{\theta_s}-q_r\right),\quad f=2\Omega\sin\varphi,\quad \tilde{f}=2\Omega\cos\varphi,$$

$$\frac{\partial \theta' p_*}{\partial t}+\frac{\partial u\theta' p_*}{\partial x}+\frac{\partial v\theta' p_*}{\partial y}+\frac{\partial \dot{\sigma}\theta' p_*}{\partial \sigma}=-S_v\tilde{w}p_*\frac{\partial \theta_s}{\partial \sigma}+p_*F_{rad}+$$

$$+p_*\frac{L_v}{c_p}\left(\frac{p_0}{p}\right)^k(C-E)+p_*D_\theta.$$

Turbulent closure

$$\frac{\partial u_i}{\partial t} = -\frac{\partial u_i u_j}{\partial x_j} - \frac{\partial p}{\partial x_i} + \frac{1}{Re}\frac{\partial^2 u_i}{\partial x_i \partial x_j} + F_i^e,$$

$$\frac{\partial u_i}{\partial x_i} = 0,$$

Navier-Stokes equations.
Approximate form of the momentum and mass conservation laws in viscous incompressible fluid.

$$F(a(x,t)) \equiv \overline{a}(x,t) = \int_{R^3} G(x-x', \Delta_f)a(x',t)dx'$$

$$\overline{\frac{\partial a(x,t)}{\partial x_i}} = \frac{\partial \overline{a}(x,t)}{\partial x_i}; \quad \overline{\frac{\partial a(x,t)}{\partial t}} = \frac{\partial \overline{a}(x,t)}{\partial t}$$

Spatial filtering
It's usually assumed that filter commutes with operator of differentiation.
It's not always the case near the boundary and/or after discretization

LES

$$\frac{\partial \overline{u}_i}{\partial t} = -\frac{\partial \overline{u}_i \overline{u}_j}{\partial x_j} - \frac{\partial \tau_{ij}}{\partial x_j} - \frac{\partial \overline{p}}{\partial x_i} + \frac{1}{Re}\frac{\partial^2 \overline{u}_i}{\partial x_i \partial x_j} + \overline{F_i^e},$$

$$\frac{\partial \overline{u}_i}{\partial x_i} = 0,$$

$$\tau_{ij} = \overline{u_i u_j} - \overline{u_i}\ \overline{u_j}.$$

Re-independent statistics of large-scale motions in turbulent flows (*observation and high-Re DNS data*) gives us hope of possibility:

1. To neglect the viscous term.

2. To find closure:
$$\tau_{ij} \approx \mathrm{T}_{ij}(\overline{u}_k, \overline{u}_l, \overline{u}_m)$$

Central problem of LES modeling. Universal approach isn't known.

The most difficult in anisotropic wall-bounded flows
(if the energy production range isn't strongly separated from dissipation range and/or inertial range can't be resolved by the numerical model)

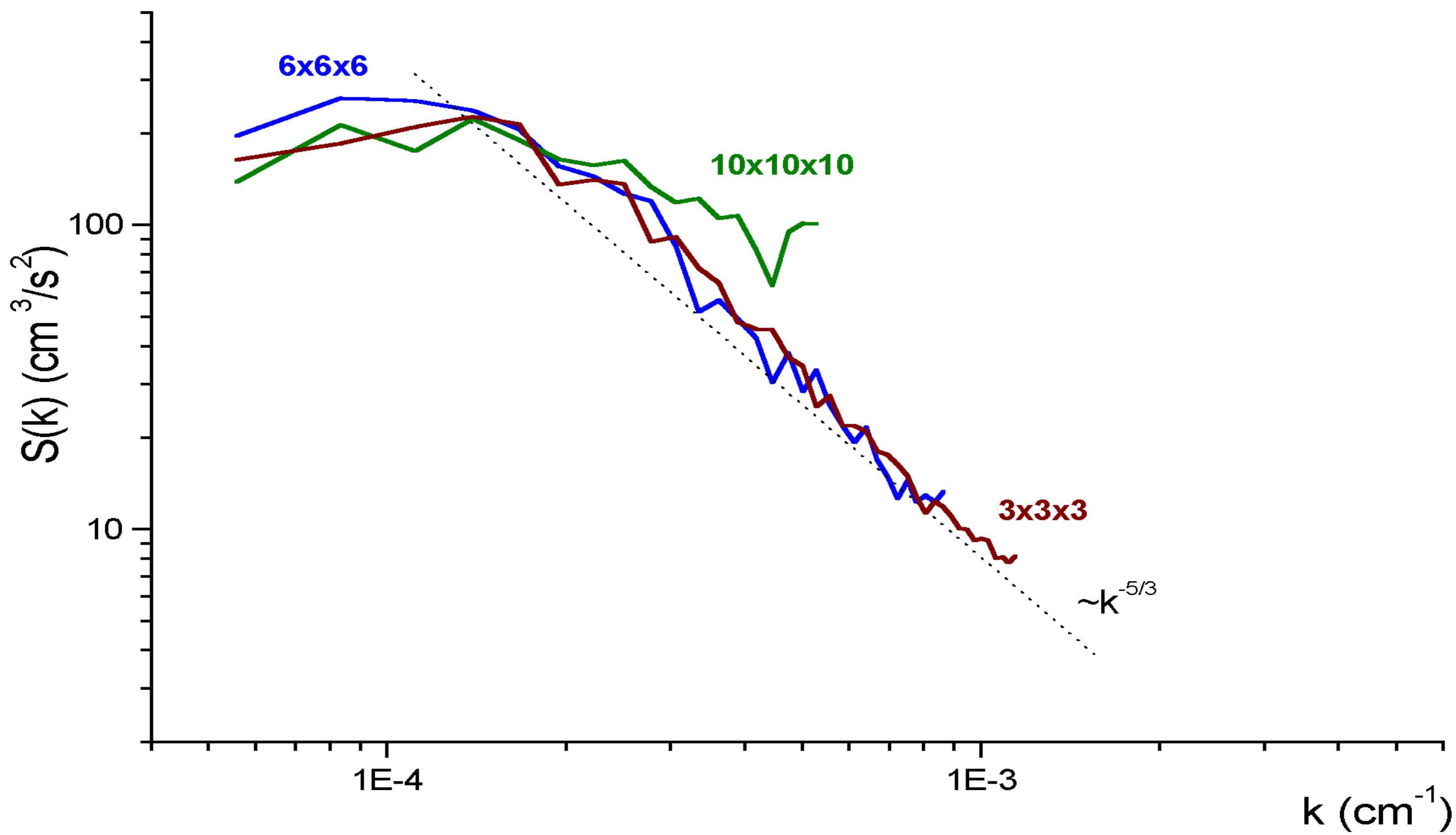

Spectra of kinetic energy calculated using results of large-eddy simulation of the convective upper oceanic layer under different spatial resolution (m^3)

A.V. Glazunov, V.P. Dymnikov, V.N. Lykosov. Mathematical modeling of spatial spectra of atmospheric turbulence. - Submitted to Russian Journal of Numerical Analysis and Mathematical Modeling.

The Rayleigh - Bernard thermal convection in a double-periodic channel with firm walls is investigated, using a LES model, as analogue of multi-scale atmospheric turbulence from the point of view of reproduction of spectral properties.

The large ratio of its horizontal size to the vertical has provided existence of a quasi-two-dimensional large-scale flow component, and the size of a uniform finite-difference grid in some tens millions points has allowed to reproduce explicitly dynamics of a small-scale three-dimensional turbulent component.

Decomposition of studied turbulent flow on barotropic and baroclinic components has allowed to offer the scheme of transformations of kinetic energy in the studied system, explaining some spectral properties of observed atmospheric turbulence.

$$\frac{\partial \bar{u}_i}{\partial t} = -\frac{\partial \overline{u_i u_j}}{\partial x_j} - \frac{\partial \bar{p}}{\partial x_i} + \delta_{i3}\alpha\left(\bar{\theta} - \left\langle \bar{\theta} \right\rangle_{x_1 x_2}\right),$$

$$\frac{\partial \bar{u}_i}{\partial x_i} = 0, \quad \frac{\partial \overline{u_i u_j}}{\partial x_j} = \frac{\partial \bar{u}_i \bar{u}_j}{\partial x_j} + \frac{\partial \boldsymbol{\tau}_{ij}}{\partial x_j}, \quad \boldsymbol{\tau}_{ij} = L_{ij}^g + C_{ij}^g + R_{ij}^g,$$

$$L_{ij}^g = \boldsymbol{\tau}^g(\bar{u}_i, \bar{u}_j),$$

$$C_{ij}^g = \boldsymbol{\tau}^g(\bar{u}_i, u_j') + \boldsymbol{\tau}^g(\bar{u}_j, u_i'),$$

$$R_{ij}^g = \boldsymbol{\tau}^g(u_i', u_j'),$$

$$\frac{\partial}{\partial x_j}\left(C_{ij}^g + R_{ij}^g\right) = -\frac{\partial}{\partial x_j}\left(2K_u \bar{S}_{ij}\right),$$

$$\frac{\partial \bar{\theta}}{\partial t} = -\frac{\partial \bar{u}_i \bar{\theta}}{\partial x_i} + \frac{\partial}{\partial x_i} K_\theta \frac{\partial \bar{\theta}}{\partial x_i}.$$

$$\varphi(x_1+L_1,x_2+L_2,x_3)=\varphi(x_1,x_2,x_3),\quad L_1:L_2:L_3=25{,}6:25{,}6:1.$$

$$u_3=0 \quad \text{at} \quad x_3=0 \wedge x_3=L_3,$$

$$\tau_{i3}(x_1,x_2,0)=-C_D(U\overline{u}_i)_{x_3=\Delta x/2},$$

$$\tau_{i3}(x_1,x_2,L_3)=C_D(U\overline{u}_i)_{x_3=L_3-\Delta x/2},$$

$$\overline{u_3'\theta'}(x_1,x_2,0)=\overline{u_3'\theta'}(x_1,x_2,L_3)=H=\text{ const.}$$

$$\overline{\mathrm{u}}(\mathrm{x},t=0)=0,$$

$$\left\langle\overline{\theta}\right\rangle_{x_1x_2}(x_3,t=0)=\text{const},$$

$$\overline{\theta}(\mathrm{x},t=0)=\left\langle\overline{\theta}\right\rangle_{x_1x_2}(x_3,t=0)+\text{ noise.}$$

Spatial resolution: 1024 x 1024 x 40 = 41 943 040 grid points.

Temperature anomalies at z=L3/8 calculated in Exp. 1 (Cd=0) for different moments of time (from left to right and from top to down)

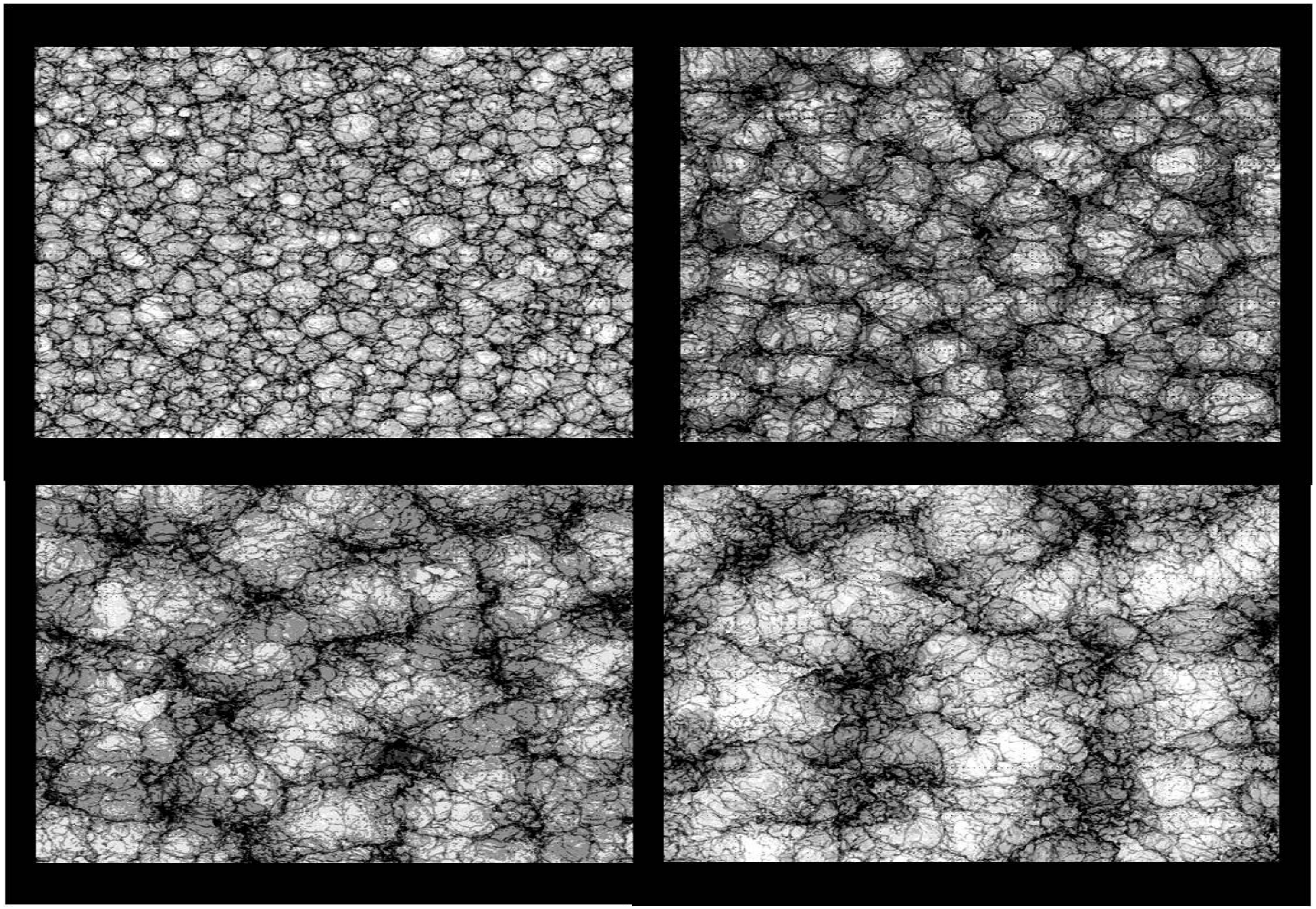

$$\frac{\partial}{\partial t}\frac{1}{2}\overline{u}_3^2 = \alpha\left(\overline{\theta} - \left\langle \overline{\theta} \right\rangle_{x_1 x_2}\right)\overline{u}_3 + \ldots$$

$$\mathrm{C}_{\theta u_3} = \mathrm{Re}\left[\hat{u}_3(\mathrm{k})\hat{\theta}^*(\mathrm{k})\right]$$

$$|\,k_{12}\,|\,C_{\theta u_3}(|\,k_{12}\,|), \quad \left|k_{12}\right| = \sqrt{k_1^2 + k_2^2}$$

Decomposition on barotropic and baroclinic components:

$$\tilde{u}_i = F^{bt}u_i \equiv \frac{1}{L_3}\int_0^{L_3} u_i dx_3, \quad (i = 1,2),$$

$$\tilde{u}_3 = 0,$$

$$u_i^{bc} = u_i - \tilde{u}_i$$

Co-spectra of temperature anomalies and vertical velocity for different moments of time

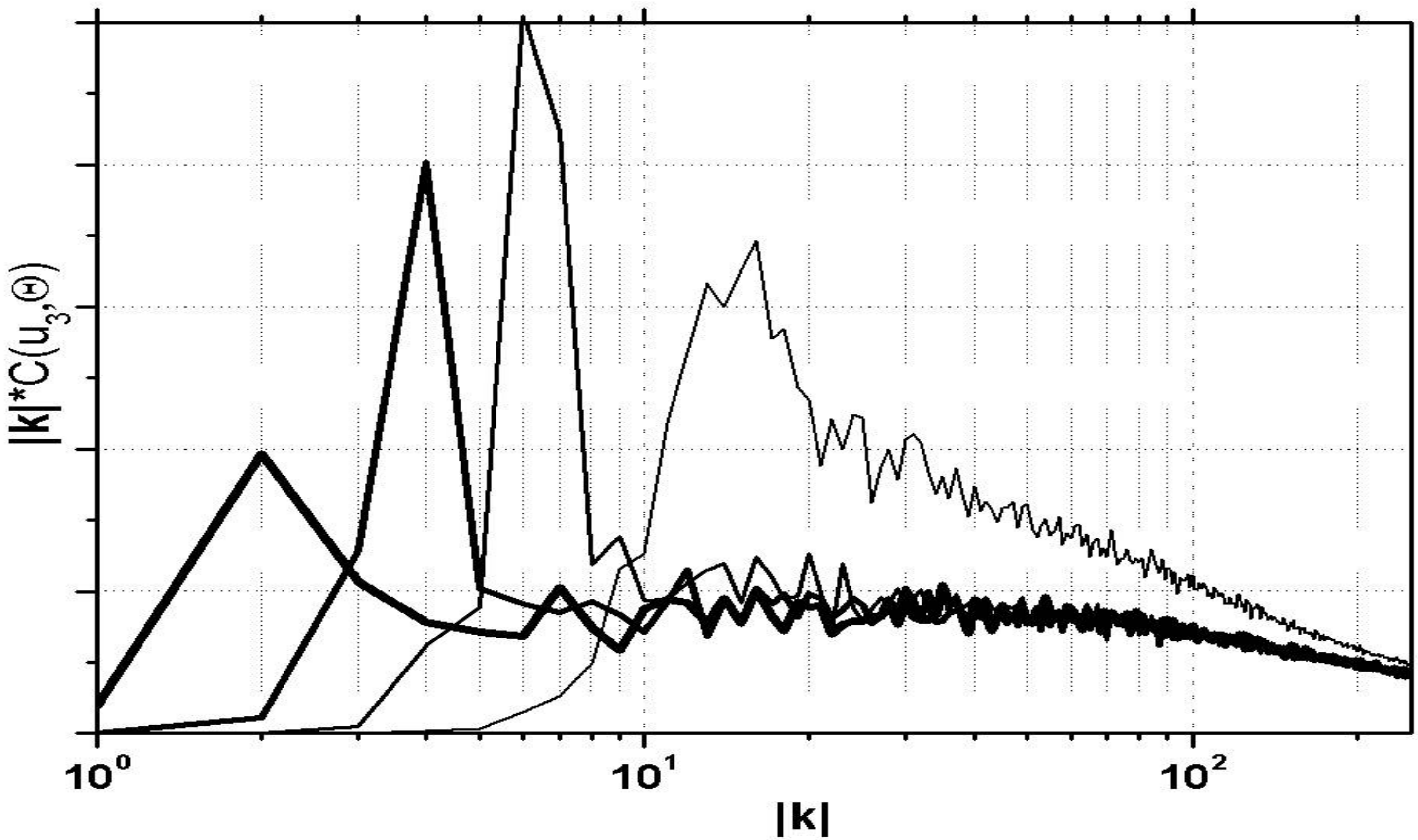

Streamlines for barotropic (left) and baroclinic (right) components of flow

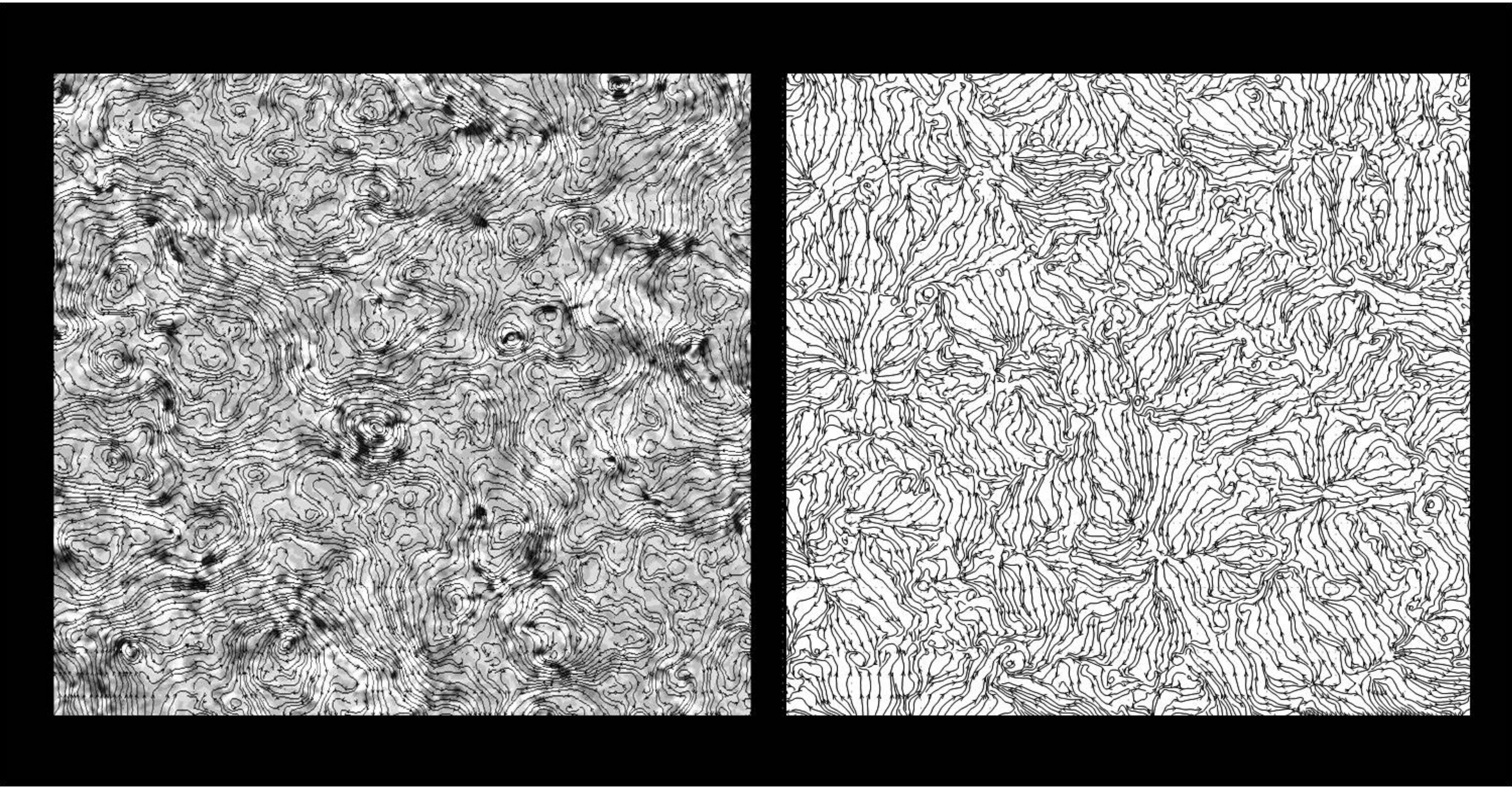

Scheme of transformations of kinetic energy

- **Kinetic energy arrives at the expense of transformation of available potential energy to baroclinic kinetic energy (through the vertical velocity) on scale of large thermals and is redistributed on the same scale through the pressure gradient in baroclinic components related to horizontal components of the wind velocity.**
- **At the expense of nonlinear interactions the baroclinic energy is transported towards small scales, forming the inertial interval with the spectral distribution close to the law "-5/3" (arrow 1).**
- **In the range of scales close to vertical size of domain, there is an essential reorganisation of baroclinic fluctuations of the wind velocity, providing transformations of energy from barotropic part to baroclinic one and back with positive, on the average, contribution to energy of the vertically averaged flow.**

One-dimensional energy spectra of stream velocity pulsations (baroclinic and barotropic components)

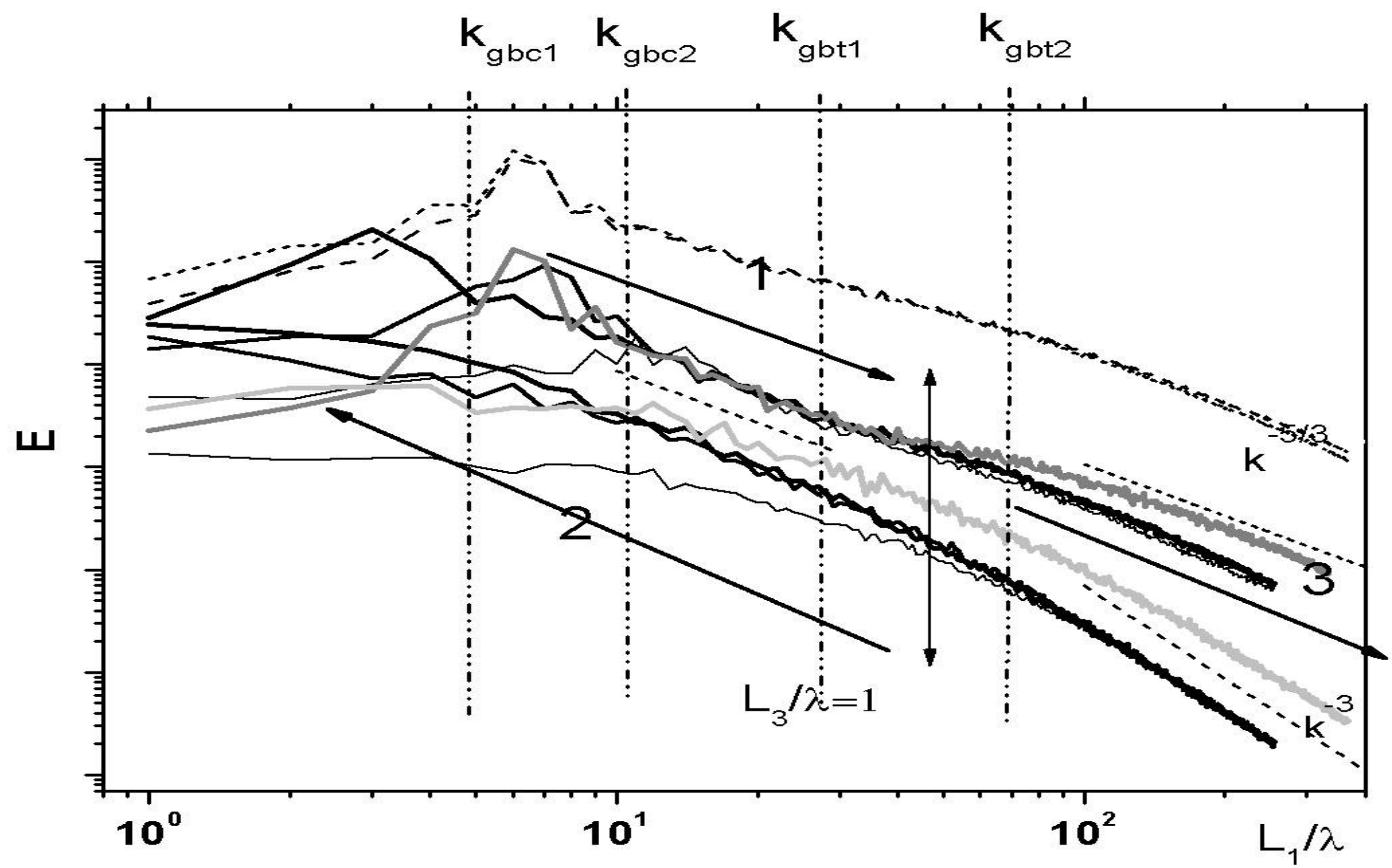

Scheme of transformations of kinetic energy (cont.)

- **Energy of the barotropic component propagates from its source, basically, towards large scales, forming spectral dependence $E_{\theta\%}: k^{-5/3}$ (arrow 2) , and also, to a lesser degree, towards small scales and this due to the enstrophy cascade leads to distribution $E_{\theta\%}: k^{-3}$ (arrow 3).**
- **The rest of baroclinic kinetic energy, which is not transformed to a barotropic component, is transferred through the direct cascade of nonlinear interactions towards small scales (arrow 3), where is dissipeared (in the case of LES-model, due to dissipative contribution of a turbulent closure, and in the case of a real turbulent flow - at the expense of forces of molecular viscosity).**
- **The account of the boundary friction does not change essentially qualitative picture of the convection development except that instead of large Bernard cells the longitudinal large-scale rolls can be formed.**

One-dimensional energy spectra of stream velocity pulsations (baroclinic and barotropic components)

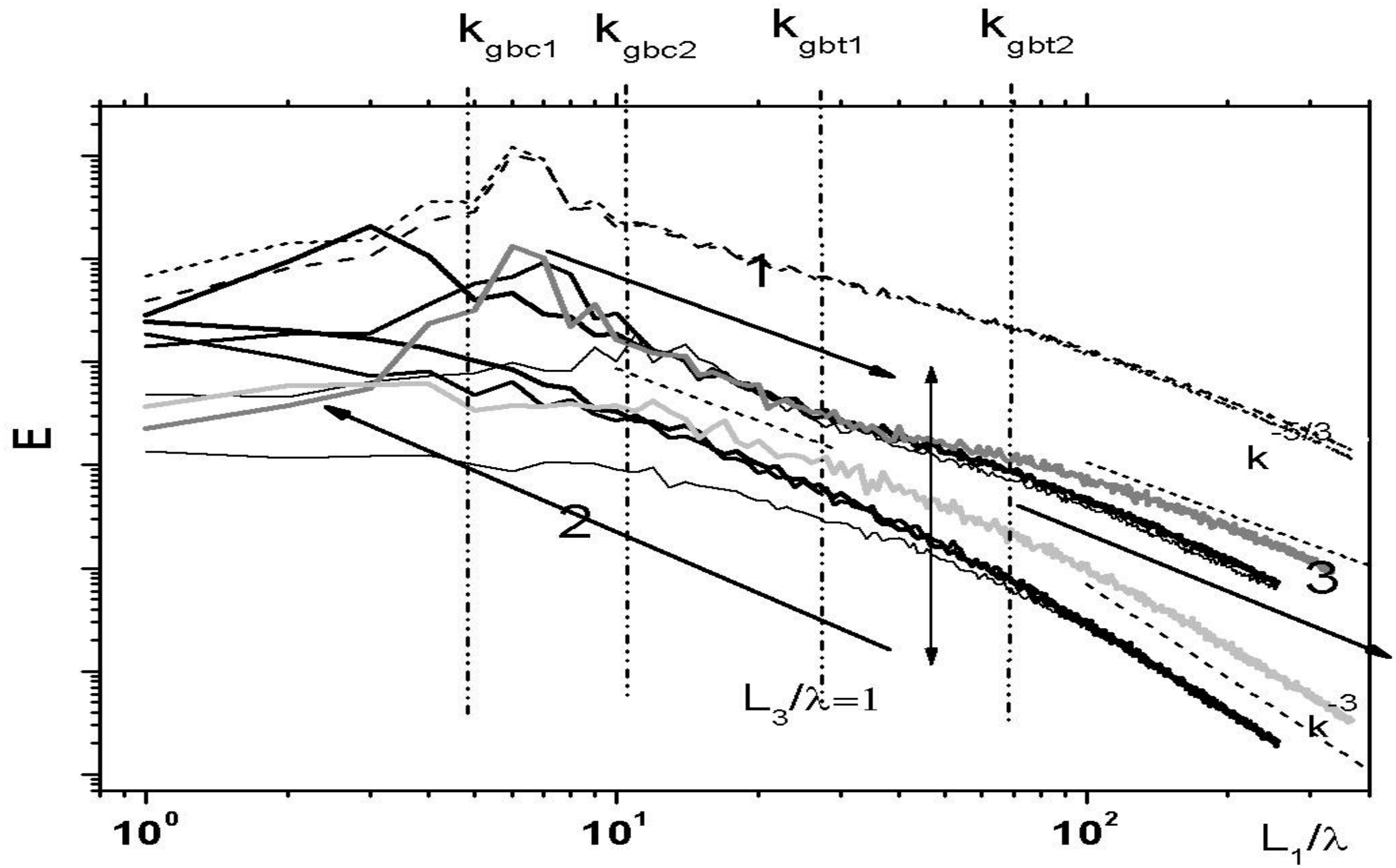

Spectra of the energy for barotropic and baroclinic flow components
(role of the boundary stress)

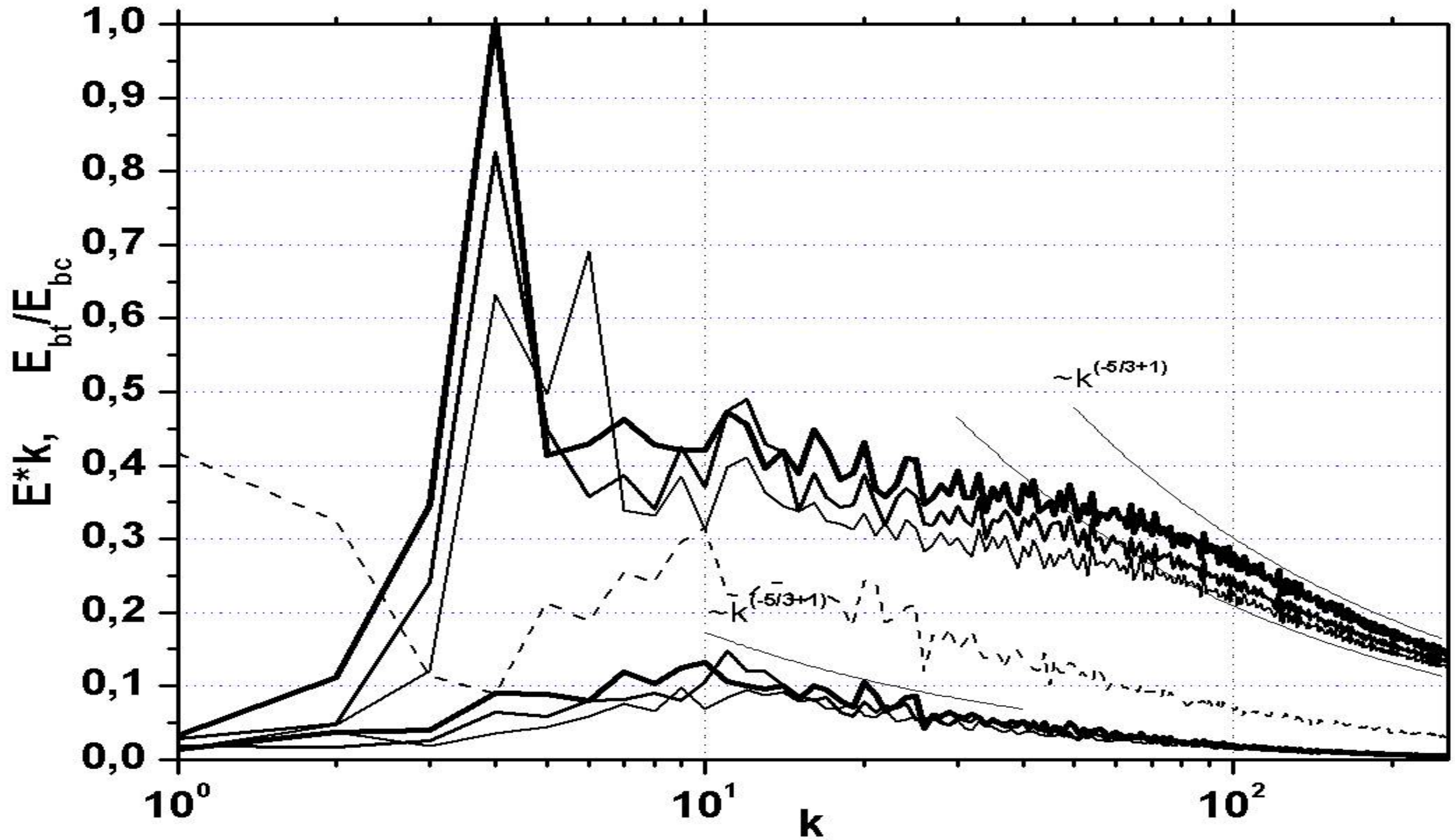

Summary

1. The further development of climate models requires an explicit description of mesoscale processes (resolution, detailed representation of inhomogeneous underlying surface, etc.).
2. It means that the hydrostatic approximation should be replaced by the non-hydrostatic formulation.
3. New parameterizations of subgrid-scale processes should be developed (e.g., accounting for secondary circulations, stochastic processes, etc.).
4. In particular, the question on what large-scale structures are formed and how the surface friction influences their formation, is important for understanding and parameterization of momentum, heat and moisture transport in the atmospheric boundary layer.
5. The computational “environment” should be also revisited: numerical schemes (unstructured grids, in time - explicit, semi-implicit or fully implicit?), parallel algorithms, effective implementation on multi-processor computational systems, etc.

THANK YOU

FOR YOUR ATTENTION!